

pubs.acs.org/JPCL Letter

A Free Energy Decomposition Analysis: Insight into Binding Thermodynamics from Absolutely Localized Molecular Orbitals

Justin J. Talbot,* Romit Chakraborty, Hengyuan Shen, and Martin Head-Gordon*



Cite This: J. Phys. Chem. Lett. 2023, 14, 5432-5440



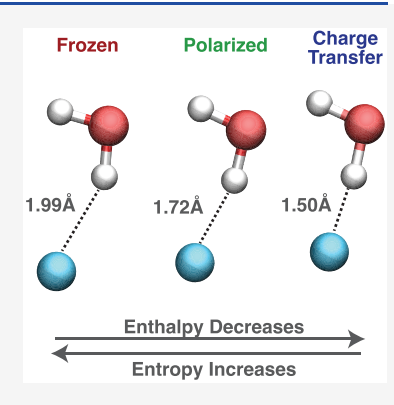
ACCESS I

III Metrics & More

Article Recommendations

s Supporting Information

ABSTRACT: Traditional energy decomposition analysis (EDA) methods can provide an interpretive decomposition of non-covalent electronic binding energies. However, by definition, they neglect entropic effects and nuclear contributions to the enthalpy. With the objective of revealing the chemical origins of trends in free energies of binding, we introduce the concept of a Gibbs decomposition analysis (GDA) by coupling the absolutely localized molecular orbital treatment of electrons in non-covalent interactions with the simplest possible quantum rigid rotor—harmonic oscillator treatment of nuclear motion at finite temperature. The resulting pilot GDA is employed to decompose enthalpic and entropic contributions to the free energy of association of the water dimer, fluoride—water dimer, and water binding to an open metal site in the metal—organic framework Cu(I)-MFU-4l. The results show enthalpic trends that generally track the electronic binding energy and entropic trends that reveal the increasing price of loss of translational and rotational degrees freedom with temperature.



he very high strength of electronic binding plays a critical role in defining the structural properties of molecules, such as chemical bonds, which are stable up to temperatures of over 1000 K. As electronic binding weakens from bonded interactions to nonbonded interactions, for fixed T, thermodynamically stable states are increasingly influenced by nuclear motion, i.e., translational, rotational, and vibrational degrees of freedom (DOF). For instance, small-molecule drug binding to protein receptors is often dominated by non-covalent interactions resulting in many thermodynamically accessible binding configurations even at relatively low temperatures. 1-5 With current developments in renewable energy and atmospheric technologies, computationally tractable models of binding free energies are essential tools used in the molecular engineering of adsorbent frameworks for gas sequestration and trapping.6-

Energy decomposition analysis (EDA) methods decompose the electronic binding energy and other properties into physically meaningful and chemically intuitive components. On the absolutely localized molecular orbital (ALMO) EDA between two fragments. Using Kohn—Sham density functional theory (DFT), ALMO-EDA augments the initial and final energies with two other intermediate energies that are minimized subject to a set of progressively weaker constraints on the one-particle density matrix (1PDM). The details of the ALMO-EDA method are outlined in the Supporting Information and are also fully described elsewhere. Information and are also fully described elsewhere.

In ALMO-EDA, the electronic binding energy is recast from a simple energy difference into a sum of physically

interpretable terms defined via the intermediate constrained

$$\Delta E_{\text{bind}} = E_{\text{FULL}} - \sum_{A} E_{A}$$

$$= \Delta E_{\text{GD}} + \Delta E_{\text{FRZ}} + \Delta E_{\text{POL}} + \Delta E_{\text{CT}}$$
(1)

The first term denotes the geometric distortion (GD) of fragments to the geometry that they adopt in the complex. The second term is the frozen interaction (FRZ), which physically is the sum of permanent electrostatics, Pauli repulsion, and dispersion. $\Delta E_{\rm FRZ}$ is the energy difference between the frozen energy $E_{\rm FRZ}$, evaluated with the very strong constraint of using the frozen orbitals of the fragments, and the sum of the isolated (distorted) fragment energies. The next term denotes the energy lowering due to polarization (POL) and is defined as the energy difference between the polarization energy, $E_{\rm POL}$, which is evaluated with the weaker constraint of allowing self-consistent on-fragment relaxation, and the frozen energy. Finally, the energy decrease due to charge transfer (CT) is defined as the energy difference between the fully optimized electronic energy, $E_{\rm FULL}$, and the polarization energy.

Received: May 21, 2023 Accepted: June 5, 2023 Published: June 7, 2023





Traditionally, ALMO-EDA is performed at a single complex geometry (e.g., the optimal geometry on the fully relaxed electronic surface), which may be called a vertical EDA. Alternatively, an adiabatic version³¹ of ALMO-EDA shows that energy differences from optimal configurations on each of the EDA component surfaces allow one to analyze the structural rearrangements that occur under the ALMO constraints.³² This gives a sequence of coupled electronic and structural relaxations from the isolated fragment to the final complex:

$$\Delta E_{\rm bind} = \Delta E_{\rm FRZ}^{\rm ad} + \Delta E_{\rm POL}^{\rm ad} + \Delta E_{\rm CT}^{\rm ad}$$
 (2)

An illustration highlighting the adiabatic ALMO-EDA approach is shown in Figure 1 for the water fluoride ion

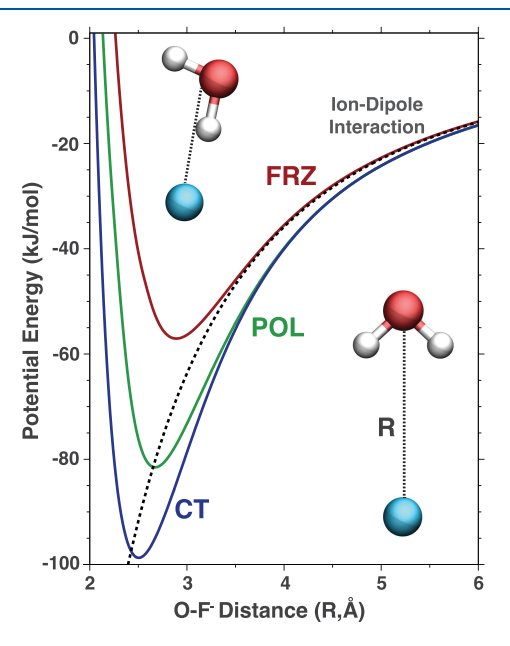


Figure 1. HF/def2-SVPD relaxed potential energy surfaces of the water fluoride ion (HOH···F $^-$). Shown are the frozen (FRZ, red), polarized (POL, green), and charge transfer (CT, blue) components of the potential energy surface as functions of the oxygen–fluoride bond length (R). The ion–dipole interaction with the water dipole calculated at the same level of theory is shown as a dashed line.

(HOH···F¯), which is a prototypical model of ion—water bonding. $^{33-38}$ The ALMO-EDA curves were calculated from geometry optimizations at the HF/def2-SVPD level of theory, constraining the oxygen fluoride distance (R). As can be seen from the figure, the minimum-energy bond length on each EDA curve is lengthened as the CT, POL, and FRZ constraints are enforced. The minimum energy on the FRZ surface occurs at $\Delta E_{\rm FRZ} = -57.1$ kJ/mol, followed by an energy decrease of $\Delta E_{\rm POL} = -24.5$ kJ/mol when POL is included, and finally, the energy lowering from CT gives an additional $\Delta E_{\rm CT} = -17.2$ kJ/mol to the bond energy. At short range ($R \lesssim 3.5$ Å) the water is preferentially hydrogen-bonded to the fluoride ion. At longer bond lengths ($R \lesssim 3.5$ Å), however, the FRZ surface follows closely the ion—dipole interaction energy. Geometrically, this results in the water preferentially aligning its dipole with the fluoride ion.

The vertical and adiabatic EDAs are powerful tools and have become quite widely used. ^{39–46} However, there is a clear gap between the physical information provided and the thermodynamic quantities ΔH , ΔS , and ΔG that control equilibrium states at any given temperature. Understanding the contribu-

tion of physical driving forces for binding in the association processes could be greatly enhanced if their influence on the trade-offs between enthalpy and entropy could also be probed. The goal of this Letter is to move in that direction by defining a free energy or Gibbs energy decomposition analysis (GDA). To pilot this idea, we shall adopt the simplest possible model for the temperature-dependent contributions of the nuclear degrees of freedom by using free translational and rigid rotor–harmonic oscillator (RR–HO) partition functions for ideal gas-phase molecules. We shall also neglect the contribution of any electronic excited states (an excellent approximation for the examples considered later).

The GDA using translational and RR-HO partition functions yields analytical expressions for thermodynamic functions given as input the equilibrium geometries and force constants on a potential surface. Further details are provided in the Supporting Information, but briefly, the Gibbs free energy of binding is

$$\Delta G_{\rm bind} = G_{\rm FULL} - \sum_{\rm A} G_{\rm A} \tag{3}$$

where $G_{\rm FULL}$ is the free energy of the interacting complex and $G_{\rm A}$ is the free energy of each isolated fragment. In the Gibbs (N,P,T) ensemble, the free energy is $G\equiv H-TS$, where H is the enthalpy, T is the temperature, and S is the entropy. If the optimal geometries and force constants are also provided on the intermediate frozen and polarized energy surfaces, we obtain thermodynamic functions corresponding to $G_{\rm FRZ}$ and $G_{\rm POL}$. In combination with $G_{\rm FULL}$ and $\{G_{\rm A}\}$, we can generate the Gibbs analogue of eq 2:

$$\Delta G_{\text{bind}} = \Delta G_{\text{FRZ}} + \Delta G_{\text{POL}} + \Delta G_{\text{CT}} \tag{4}$$

Expressions for the various thermodynamic functions in the RR–HO approximation are provided in the Supporting Information.

The ALMO-EDA free energy decomposition of the water fluoride ion is shown in Figure 2. The decomposition of the binding energy was evaluated for the histogram plots at $T=300~\rm K$ and a pressure p=1 bar. Unsurprisingly, the overwhelming contribution to the binding enthalpy (Figure 2e) comes from the electronic DOF (Figure 2b). As a result, the total binding enthalpy is systematically strengthened as the ALMO constraints are released. If the electronic contribution is removed from the binding enthalpy (i.e., $\Delta E - \Delta H$), then the nuclear DOF reduce the binding strength by 4.22 kJ/mol for the FRZ term, by 3.69 kJ/mol for the POL term, and by only 1.09 kJ/mol for the CT term. These nuclear contributions are ZPE-dominated, and the smaller CT contribution is associated with the CT-induced red shift of the OH stretch of the proton donor.

The GDA (i.e., the contributions to eq 4) at 300 K is shown in Figure 2c. ΔG for this interaction is dominated by permanent and induced electrostatics. Relative to ΔH , the importance of charge transfer is increased in ΔG . This is mainly because the dominant entropic contribution $(-T\Delta S)$ is the translational component (see Table 1). $-T\Delta S_{\text{trans}}$ is due to loss of three free translations as an effect of association, and this +41.0 kJ/mol (at 300 K) must be paid at the level of the frozen interaction. It is then identical on each subsequent electronic surface. On the other hand, the $-T\Delta S$ contributions due to the rotational and vibrational DOF increase slightly as the constraints are enforced, consistent with tighter binding. As shown in Figure 2d,g, the free energy and

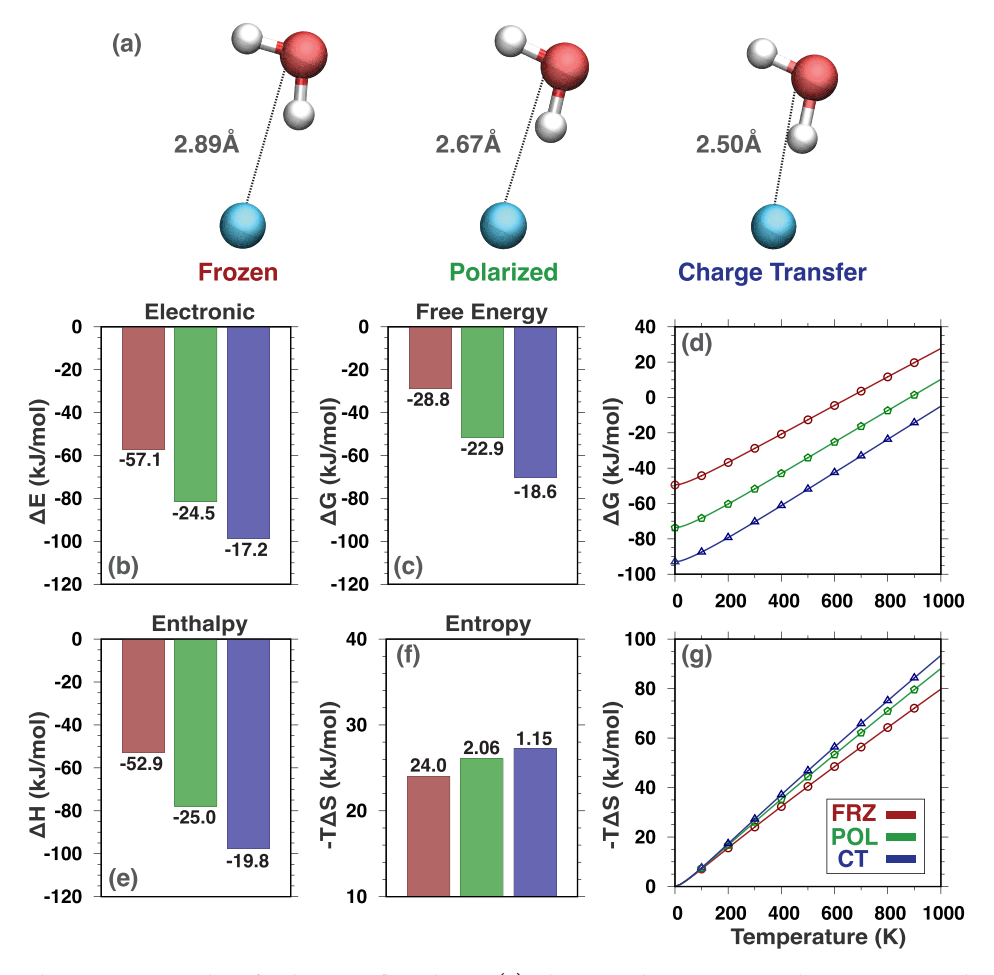


Figure 2. Free energy decomposition analysis for the water fluoride ion. (a) The optimal geometries on the FRZ, POL, and CT surfaces with the oxygen—fluoride bond length (R) are shown for reference. (b) Adiabatic ALMO-EDA components of the electronic binding energy. (c) Gibbs free energy of binding at T = 300 K and p = 1 bar. (d) Gibbs free energy of binding as a function of temperature. (e) Binding enthalpy at T = 300 K and p = 1 bar. (g) Binding entropy ($-T\Delta S$) as a function of temperature. All energies are expressed in kJ/mol. The Δ values are shown for reference under each histogram.

Table 1. Comparison between the Enthalpic and Entropic Components of the Binding Free Energy under the FRZ, POL, and CT Constraints for the Different Model Systems Analyzed in This Work^a

	H_2O-F^-			H_2O-H_2O			$Cu(I)$ -MFU-4 l - H_2O		
component	FRZ	POL	СТ	FRZ	POL	СТ	FRZ	POL	CT
Bond Enthalpy									
translations	-3.74	-3.74	-3.74	-1.25	-1.25	-1.25	-1.87	-1.87	-1.87
rotations	0.00	0.00	0.00	-1.25	-1.25	-1.25	-1.87	-1.87	-1.87
vibrations	10.5	9.92	7.33	8.07	8.55	9.45	7.96	8.98	9.57
electronic	-57.1	-81.5	-98.7	-11.0	-13.3	-19.4	-11.8	-24.7	-29.7
total	-52.9	-77.8	-97.6	-6.27	-8.06	-13.3	-8.86	-20.7	-25.1
Bond Entropy:									
translations	41.0	41.0	41.0	11.4	11.4	11.4	19.6	19.6	19.6
rotations	-12.3	-11.8	-11.4	-1.02	-0.954	-0.839	5.19	5.19	5.19
vibrations	-4.72	-3.12	-2.35	-1.84	-1.65	-1.22	-6.76	-5.26	-5.26
total	24.0	26.1	27.2	8.50	8.75	9.30	17.9	19.5	19.5

[&]quot;All enthalpies and entropies were calculated at p=1 bar and T=300 K for the water fluoride ion, T=100 K for the water dimer, and T=150 K for the MOF—water system. All values are expressed in kJ/mol.

entropy depend linearly on the temperature for $T\gtrsim 200$ K. The net effect of polarization can be viewed as raising the temperature at which $K\sim 1$ by roughly 200 K, while the effect of CT is smaller, raising the temperature at which $K\sim 1$ by roughly 150 K.

The water dimer is the prototypical model of hydrogen bonding, with many experimental and theoretical studies dedicated to decomposing the various bonding interactions. The hydrogen bond strength between two water monomers is ~ 20 kJ/mol, where the minimum-energy configuration is a near-linear geometry with a single hydrogen

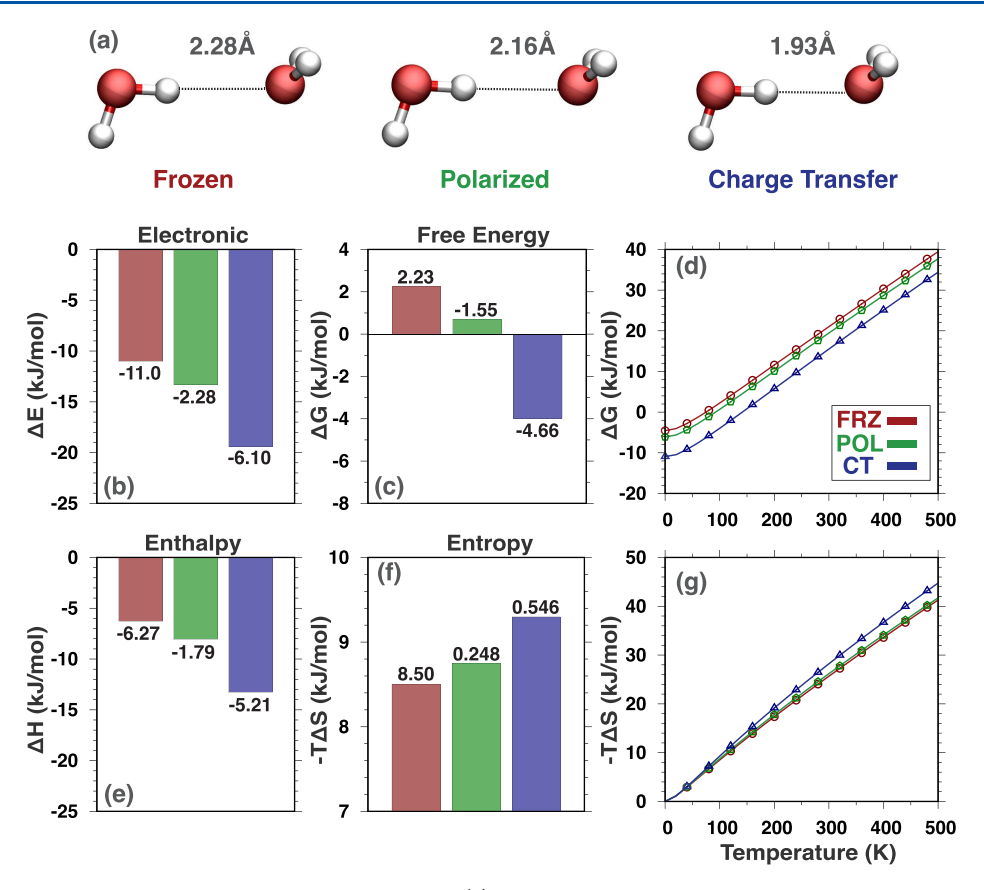


Figure 3. Free energy decomposition analysis for the water dimer. (a) The optimal geometries on the FRZ, POL, and CT surfaces with the hydrogen—oxygen bond length are shown for reference. (b) Adiabatic ALMO-EDA components of the electronic binding energy. (c) Gibbs free energy of binding at T = 100 K and p = 1 bar. (d) Gibbs free energy of binding as a function of temperature. (e) Binding enthalpy at T = 100 K and p = 1 bar. (g) Binding entropy ($-T\Delta S$) as a function of temperature. All energies are expressed in kJ/mol. The Δ values are shown for reference under each histogram.

bond connecting the two monomers.⁵⁸ The ALMO-EDA free energy decomposition, using the B3LYP/def2-SVPD level of theory, is shown in Figure 3 at T = 100 K and p = 1 bar. For the water dimer, the enthalpic contributions to binding from the nuclear DOF play a more significant role than for water fluoride ion since the electronic contribution to binding is substantially smaller. If the electronic binding enthalpy is again removed (i.e., $\Delta H - \Delta E$), the nuclear DOF reduces binding by 4.74 kJ/mol for the FRZ term, by 5.23 kJ/mol for the POL term, and by 6.12 kJ/mol for the CT term. As a result, even at 100 K, the entropy contribution overtakes the enthalpy on the FRZ free energy surface, and the binding free energy is unfavorable (i.e., $\Delta G_{FRZ} = +2.23$ kJ/mol). Additionally, since POL does not increase binding sufficiently, the entropic contribution also unbinds the two fragments on the POL surface (i.e., $\Delta G_{POL} = +0.689$ kJ/mol). Only when CT is included is the association of two water molecules favorable at 100 K (i.e., $\Delta G_{\text{FULL}} = -3.97 \text{ kJ/mol}$).

Coordinatively unsaturated open metal sites in metal-organic frameworks (MOFs) have been utilized as an adsorbent for small-molecule gas sequestration and trapping. Typically, binding of an adsorbate to an open metal site in these systems is dominated by physisorption (van der Waals interactions) due to embedding of the binding site, which acts to hinder strong adsorption; however, recent studies have focused on MOF systems that can more strongly bind (i.e., chemisorb) their target adsorbates. For instance, of the many recently synthesized MOFs that exhibit this binding

trend, the copper scorpionate-type Cu(I)-MFU-4l has been recently shown to undergo chemisorption binding to a H_2 adsorbate. Details of the cluster model employed for this work and its validation for H_2 binding to the framework can be found in ref 65.

The ALMO-EDA free energy procedure was employed to analyze the interaction of a gas-phase water adsorbate with the Cu open metal site of Cu(I)-MFU-4l using a cluster model. The electronic energy was evaluated using the ω B97M-V density functional⁶⁶ with a mixed basis of def2-TZVPPD on the water adsorbate and the Cu binding site and the def2-SVP basis used on all other atoms. Harmonic oscillator frequencies and rotation constants were calculated with the def2-SVP basis⁶⁷ at this basis set's optimal geometries. The results are shown in Figure 4 at T = 150 K and p = 1 bar. Again, if the electronic binding enthalpy is removed (i.e., $\Delta H - \Delta E$), the nuclear DOF reduces the enthalpy of binding by 2.97 kJ/mol on the FRZ surface, by 3.99 kJ/mol on the POL surface, and by 4.59 kJ/mol on the full surface. The relatively weak enthalpy of binding on the FRZ surface means that association of the two fragments at 150 K is not favorable due to the relatively large entropic binding penalty ($-T\Delta S = 18.0 \text{ kJ/mol}$; ΔG_{FRZ} = +9.12 kJ/mol). However, since the binding enthalpy increases strongly on the POL surface, association of the two fragments becomes favorable ($\Delta G_{POL} = -1.24 \text{ kJ/mol}$). Donor-acceptor interactions on the full surface make the free energy of association more favorable ($\Delta G = -5.61 \text{ kJ/}$

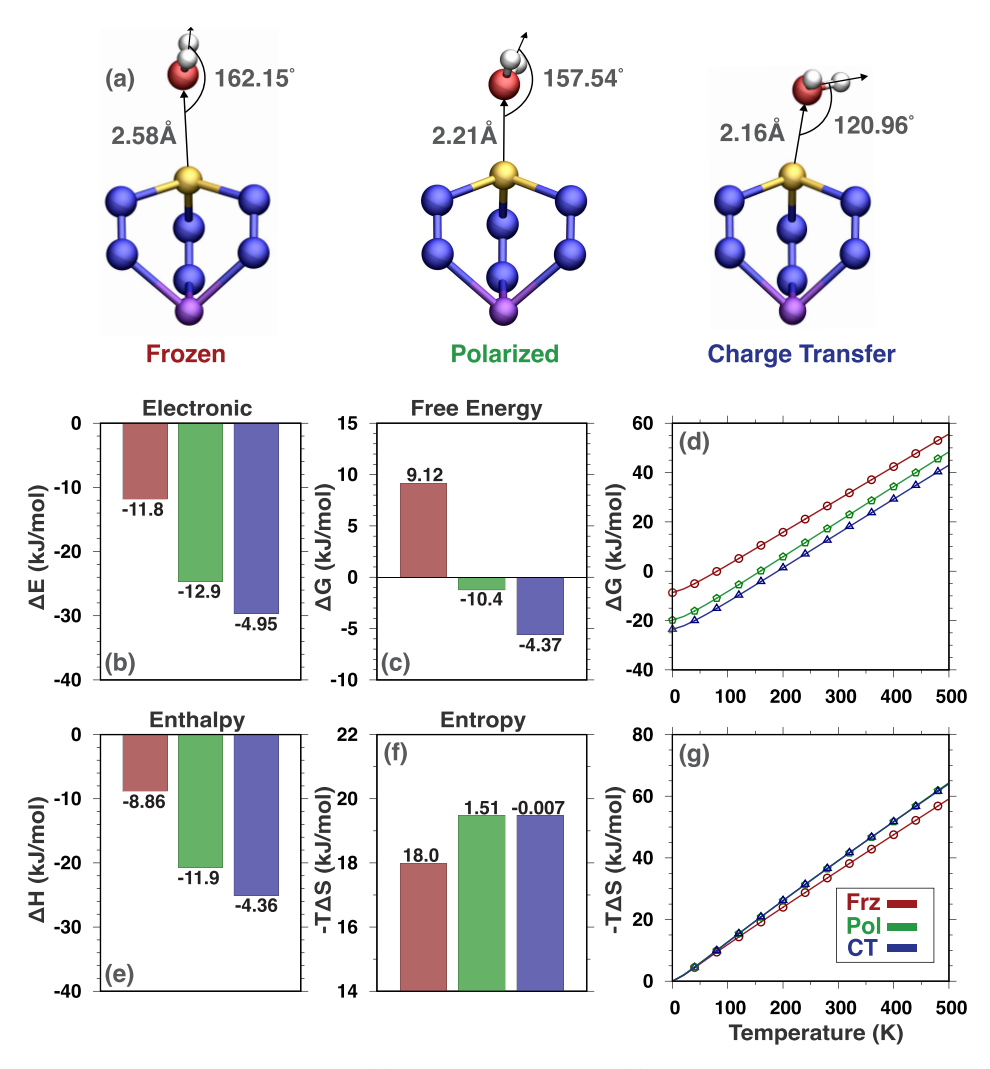


Figure 4. Free energy decomposition analysis for the Cu(I)-MFU-4l- H_2O system. (a) Optimal geometries with select atoms shown near the binding site on the FRZ, POL, and CT components of the potential energy surface. The optimal oxygen-copper bond length and angle between the oxygen-copper bond and a vector bisecting the two hydrogen atoms from the adsorbed water molecule is shown. (b) Adiabatic ALMO-EDA components of the electronic binding energy. (c) Gibbs free energy of binding at T = 150 K and p = 1 bar. (d) Gibbs free energy of binding as a function of temperature. (e) Binding enthalpy at T = 150 K and p = 1 bar. (f) Binding entropy at T = 150 K and T = 150

mol), though binding is dominated by permanent and induced electrostatics.

The dominance of electrostatics in the binding is evident in the optimized Cu-OH_2 distances, which are 2.16 Å on the full surface, 2.21 Å on the POL surface (i.e., removing dative interactions), and 2.58 Å on the FRZ surface (i.e., removing induced electrostatics as well as CT). While the CT contribution to binding is secondary, it does have a dramatic effect on the angle between the copper—oxygen bond and a vector bisecting the two hydrogen atoms on the water, as shown in Figure 4. On the FRZ and POL surfaces, the dipole of the water molecule nearly aligns with the copper center, with angles of 162.15° and 157.54° . Upon release of all constraints, the water molecule lies almost perpendicular to the copper site at an angle of 120.96° . This is remarkable because it weakens the charge—dipole interactions that are crucial for binding.

To investigate the nature of this bonding pattern further, a complementary occupied-virtual pair (COVP) analysis was performed for both the POL and CT interactions. The results are shown in Figure 5. We may be expecting strong

polarization of the water molecule by the formally charged Cu(I) site, but this is not the main effect. Rather, at the POL level, it is the Cu center that is more strongly polarized, and the main contributing COVP (71%) describes the occupied $3d_{z^2}$ orbital of Cu mixing with an empty sp³-like hybrid orbital. The next highest contributing pair is on water: a donation from a plike lone pair (lp) orbital on oxygen into an lp*-like orbital, which accounts for an additional 14% of the POL interaction. As was found previously, the electron density increases at the places where the occupied and virtual COVPs have the same phase and vice versa. Therefore, the POL COVPs tell us that the 3d_{z²} orbital of Cu was polarized away from water by mixing with the sp-like hybrid orbital due to Pauli repulsion from the water's oxygen lone pair. On the other hand, the p electrons of oxygen polarize toward Cu to induce a larger dipole moment, as anticipated. This latter effect also serves to prepare water for the CT process. When CT is included (see Figure 5b), the main contributing COVP accounts for 67% of the interaction and can be described as a σ donation from an occupied lp orbital on water donating into an empty sp³ Cu orbital. This relatively weak CT effect is enhanced by the aforementioned

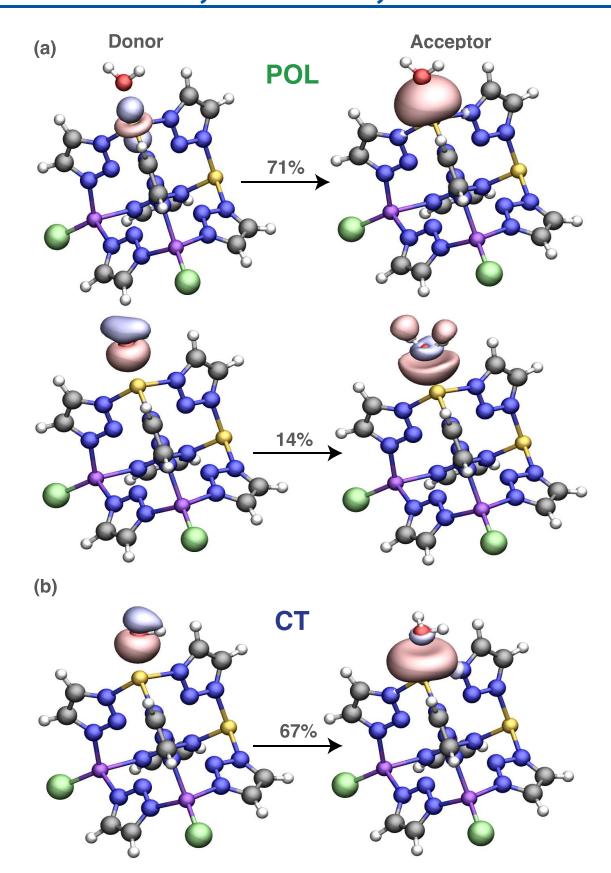


Figure 5. Leading POL and CT constrained occupied—virtual pairs (COVPs) of a gas-phase water adsorbate binding on the open-metal copper site of Cu(I)-MFU4-l. (a) The two leading POL pairs. (b) The leading CT pair. The percentage contributions to the energy are shown above the arrows. The atom color codes are gray (C), blue (N), green (Cl), purple (Zn), white (H), red (O), and gold (Cu). The COVPs were plotted with an isosurface value of ± 0.07 au.

reorientation of the water molecule, to an extent that exceeds the loss of electrostatic polarization.

A comparison between the different enthalpy and entropy components is shown in Table 1. The general trend among the model systems studied here is that releasing the ALMO-EDA constraints, from FRZ to POL to CT, strengthens the overall binding enthalpy due to the electronic contribution. Besides the electronic binding enthalpy, the only varying component is from the vibrational DOF, which decreases as the constraints are released for water fluoride but increases for all other systems analyzed. The main contributor to the binding entropy is translational confinement, which, under the approximations assumed here, is invariant under the ALMO constraints and only depends on the pressure, temperature, and mass. However, the total binding entropy $(-T\Delta S)$ follows the reverse trend to the enthalpy in that releasing the ALMO constraints systematically decreases the $-T\Delta S$ term after relaxing the constraints.

The adiabatic ALMO-EDA method³¹ enables a detailed analysis of electronic binding energies and other properties into physically meaningful components such as Pauli repulsion, dispersion, polarization, and charge transfer. Here, the adiabatic ALMO-EDA method was extended to decompose thermodynamic contributions to the free energy of association for some prototypical hydrogen-bonding motifs and to an anomalous binding motif involving a metal—organic framework

and a "flat-lying" gas-phase water adsorbate. Although the GDA approach described here decomposes the binding thermodynamics into FRZ, POL, and CT components, it is important to remember that the FRZ \rightarrow POL \rightarrow FULL sequence is purely for analysis and that binding is not a stepwise process in that sense. The only sense in which binding can be stepwise is via intermediate states, such as, in some cases, weakly bound precursors to more strongly bound states. ^{65,71}

The free energy model presented here was a simple RR-HO estimate of the various thermodynamic quantities, which has the virtue of leading to analytical expressions. However, there are also clearly some limitations to this approach. For instance, this approach assumes a separable product partition function for the translational, rotational, vibrational, and electronic DOF. Vibronic and rovibrational coupling effects as well as anharmonicities and mode coupling that arises from the vibrational DOF would likely have a significant impact on the estimates of bond energies and trends. Investigating these effects within the ALMO-EDA partition using grid-based molecular dynamics and Monte Carlo methods will be interesting topics for future work. It will also be particularly interesting to explore whether generalizations of the free energy decomposition analysis are possible for the condensed phase.

ASSOCIATED CONTENT

Supporting Information

The Supporting Information is available free of charge at https://pubs.acs.org/doi/10.1021/acs.jpclett.3c01397.

Brief derivation of the ALMO-EDA method and expressions for the Gibbs free energy, enthalpic, and entropic ALMO-EDA components in the RR–HO approximation and additional ALMO-EDA and basis set analysis on the Cu(I)-MFU-4l- H_2O model system (PDF)

AUTHOR INFORMATION

Corresponding Authors

Justin J. Talbot — Department of Chemistry, University of California, Berkeley, California 94720, United States; orcid.org/0000-0001-8895-4893; Email: justin.talbot@berkeley.edu

Martin Head-Gordon — Department of Chemistry, University of California, Berkeley, California 94720, United States; Chemical Sciences Division, Lawrence Berkeley National Laboratory, Berkeley, California 94720, United States; orcid.org/0000-0002-4309-6669; Email: mhg@cchem.berkeley.edu

Authors

Romit Chakraborty — Department of Chemistry, University of California, Berkeley, California 94720, United States; Materials Sciences Division, Lawrence Berkeley National Laboratory, Berkeley, California 94720, United States; orcid.org/0000-0002-4638-6346

Hengyuan Shen – Department of Chemistry, University of California, Berkeley, California 94720, United States; orcid.org/0000-0001-7535-600X

Complete contact information is available at: https://pubs.acs.org/10.1021/acs.jpclett.3c01397

Notes

The authors declare the following competing financial interest(s): M.H.-G. is a part-owner of Q-Chem Inc., whose software was used for the developments and calculations reported here.

ACKNOWLEDGMENTS

All authors acknowledge support from the U.S. National Science Foundation through Grant CHE-1955643. This research used resources of the National Energy Research Scientific Computing Center (NERSC), a U.S. Department of Energy Office of Science User Facility located at Lawrence Berkeley National Laboratory, operated under Contract DE-AC02-05CH11231 using NERSC Award BES-ERCAP0025080. J.J.T. acknowledges support from the National Science Foundation under Grant CHE-1856707. R.C. and M.H.-G. acknowledge additional support from the Hydrogen Materials - Advanced Research Consortium (HyMARC), established as part of the Energy Materials Network under the U.S. Department of Energy, Office of Energy Efficiency and Renewable Energy, under Contract DE-AC02-05CH11231. Calculations were performed using the Q-Chem package. 72

REFERENCES

- (1) Cournia, Z.; Allen, B.; Sherman, W. Relative Binding Free Energy Calculations in Drug Discovery: Recent Advances and Practical Considerations. *J. Chem. Inf. Model.* **2017**, *57*, 2911–2937.
- (2) Cournia, Z.; Chipot, C.; Roux, B.; York, D. M.; Sherman, W. ACS Symp. Ser. 2021, 1397, 1-38.
- (3) Boz, E.; Stein, M. Accurate Receptor-Ligand Binding Free Energies From Fast QM Conformational Chemical Space Sampling. *Int. J. Mol. Sci.* **2021**, 22, 3078.
- (4) Lu, H.; Marti, J. Cellular Absorption of Small Molecules: Free Energy Landscapes of Melatonin Binding at Phospholipid Membranes. *Sci. Rep.* **2020**, *10*, 9235.
- (5) Huang, D.; Caflisch, A. The Free Energy Landscape of Small Molecule Unbinding. *PLoS Comput. Biol.* **2011**, *7*, e1002002.
- (6) Schneemann, A.; White, J. L.; Kang, S.; Jeong, S.; Wan, L. F.; Cho, E. S.; Heo, T. W.; Prendergast, D.; Urban, J. J.; Wood, B. C.; Allendorf, M. D.; Stavila, V. Nanostructured Metal Hydrides for Hydrogen Storage. *Chem. Rev.* **2018**, *118*, 10775–10839.
- (7) Düren, T.; Bae, Y.-S.; Snurr, R. Q. Using Molecular Simulation to Characterise Metal-Organic Frameworks for Adsorption Applications. *Chem. Soc. Rev.* **2009**, *38*, 1237–1247.
- (8) Luan, B.; Elmegreen, B.; Kuroda, M. A.; Gu, Z.; Lin, G.; Zeng, S. Crown Nanopores in Graphene for ${\rm CO_2}$ Capture and Filtration. *ACS Nano* **2022**, *16*, 6274–6281.
- (9) Wang, S.; Zhou, G.; Ma, Y.; Gao, L.; Song, R.; Jiang, G.; Lu, G. Molecular Dynamics Investigation on the Adsorption Behaviors of H_2O , CO_2 , CH_4 and N_2 Gases on Calcite ($1\overline{1}$ 0) Surface. *Appl. Surf. Sci.* **2016**, 385, 616–621.
- (10) Frenking, G.; Bickelhaupt, F. M. The EDA Perspective of Chemical Bonding. In *The Chemical Bond: Fundamental Aspects of Chemical Bonding*; Wiley-VCH: Weinheim, Germany, 2014; pp 121–157
- (11) Zhao, L.; von Hopffgarten, M.; Andrada, D. M.; Frenking, G. Energy Decomposition Analysis. *Wiley Interdiscip. Rev.: Comput. Mol. Sci.* 2018, 8, e1345.
- (12) Montilla, M.; Luis, J. M.; Salvador, P. Origin-Independent Decomposition of the Static Polarizability. *J. Chem. Theory Comput.* **2021**, *17*, 1098–1105.
- (13) Aldossary, A.; Gimferrer, M.; Mao, Y.; Hao, H.; Das, A. K.; Salvador, P.; Head-Gordon, T.; Head-Gordon, M. Force Decomposition Analysis: AMethod to Decompose Intermolecular Forces

- into Physically Relevant Component Contributions. J. Phys. Chem. A 2023, 127, 1760–1774.
- (14) Mao, Y.; Loipersberger, M.; Horn, P. R.; Das, A.; Demerdash, O.; Levine, D. S.; Prasad Veccham, S.; Head-Gordon, T.; Head-Gordon, M. From Intermolecular Interaction Energies and Observable Shifts to Component Contributions and Back Again: A Tale of Variational Energy Decomposition Analysis. *Annu. Rev. Phys. Chem.* **2021**, *72*, 641–666.
- (15) Herbert, J. M. Neat, Simple, and Wrong: Debunking Electrostatic Fallacies Regarding Noncovalent Interactions. *J. Phys. Chem. A* **2021**, *125*, 7125–7137.
- (16) Phipps, M. J.; Fox, T.; Tautermann, C. S.; Skylaris, C.-K. Energy Decomposition Analysis Approaches and Their Evaluation on Prototypical Protein-Drug Interaction Patterns. *Chem. Soc. Rev.* **2015**, 44, 3177–3211.
- (17) von Hopffgarten, M.; Frenking, G. Energy Decomposition Analysis. Wiley Interdiscip. Rev.: Comput. Mol. Sci. 2012, 2, 43–62.
- (18) Su, P.; Li, H. Energy Decomposition Analysis of Covalent Bonds and Intermolecular Interactions. *J. Chem. Phys.* **2009**, *131*, 014102.
- (19) Wu, Q.; Van Voorhis, T. Direct Optimization Method to Study Constrained Systems Within Density-Functional Theory. *Phys. Rev. A* **2005**, 72, 024502.
- (20) Wu, Q.; Ayers, P. W.; Zhang, Y. Density-Based Energy Decomposition Analysis for Intermolecular Interactions With Variationally Determined Intermediate State Energies. *J. Chem. Phys.* **2009**, 131, 164112.
- (21) Glendening, E. D.; Streitwieser, A. Natural Energy Decomposition Analysis: An Energy Partitioning Procedure for Molecular Interactions With Application to Weak Hydrogen Bonding, Strong Ionic, and Moderate Donor-Acceptor Interactions. *J. Chem. Phys.* 1994, 100, 2900–2909.
- (22) Glendening, E. D. Natural Energy Decomposition Analysis: Extension to Density Functional Methods and Analysis of Cooperative Effects in Water Clusters. *J. Phys. Chem. A* **2005**, *109*, 11936–11940.
- (23) Khaliullin, R. Z.; Cobar, E. A.; Lochan, R. C.; Bell, A. T.; Head-Gordon, M. Unravelling the Origin of Intermolecular Interactions Using Absolutely Localized Molecular Orbitals. *J. Phys. Chem. A* **2007**, *111*, 8753–8765.
- (24) Horn, P. R.; Mao, Y.; Head-Gordon, M. Probing Non-Covalent Interactions With a Second Generation Energy Decomposition Analysis Using Absolutely Localized Molecular Orbitals. *Phys. Chem. Chem. Phys.* **2016**, *18*, 23067–23079.
- (25) Horn, P. R.; Sundstrom, E. J.; Baker, T. A.; Head-Gordon, M. Unrestricted Absolutely Localized Molecular Orbitals for Energy Decomposition Analysis: Theory and Applications to Intermolecular Interactions Involving Radicals. *J. Chem. Phys.* **2013**, *138*, 134119.
- (26) Phipps, M. J.; Fox, T.; Tautermann, C. S.; Skylaris, C.-K. Energy Decomposition Analysis Based on Absolutely Localized Molecular Orbitals for Large-Scale Density Functional Theory Calculations in Drug Design. *J. Chem. Theory Comput.* **2016**, *12*, 3135–3148.
- (27) Horn, P. R.; Mao, Y.; Head-Gordon, M. Defining the Contributions of Permanent Electrostatics, Pauli Repulsion, and Dispersion in Density Functional Theory Calculations of Intermolecular Interaction Energies. *J. Chem. Phys.* **2016**, *144*, 114107.
- (28) Mao, Y.; Levine, D. S.; Loipersberger, M.; Horn, P. R.; Head-Gordon, M. Probing Radical-Molecule Interactions With a Second Generation Energy Decomposition Analysis of DFT Calculations Using Absolutely Localized Molecular Orbitals. *Phys. Chem. Chem. Phys.* **2020**, 22, 12867–12885.
- (29) Levine, D. S.; Horn, P. R.; Mao, Y.; Head-Gordon, M. Variational Energy Decomposition Analysis of Chemical Bonding. 1. Spin-Pure Analysis of Single Bonds. *J. Chem. Theory Comput.* **2016**, 12, 4812–4820.
- (30) Horn, P. R.; Head-Gordon, M. Alternative Definitions of the Frozen Energy in Energy Decomposition Analysis of Density Functional Theory Calculations. *J. Chem. Phys.* **2016**, *144*, 084118.

- (31) Mao, Y.; Horn, P. R.; Head-Gordon, M. Energy Decomposition Analysis in an Adiabatic Picture. *Phys. Chem. Chem. Phys.* **2017**, *19*, 5944–5958.
- (32) Mao, Y.; Head-Gordon, M. Probing Blue-Shifting Hydrogen Bonds With Adiabatic Energy Decomposition Analysis. *J. Phys. Chem. Lett.* **2019**, *10*, 3899–3905.
- (33) Weis, P.; Kemper, P. R.; Bowers, M. T.; Xantheas, S. S. A New Determination of the Fluoride Ion-Water Bond Energy. *J. Am. Chem. Soc.* **1999**, *121*, 3531–3532.
- (34) Craig, J.; Brooker, M. On the Nature of Fluoride Ion Hydration. J. Solution Chem. 2000, 29, 879–888.
- (35) Roscioli, J. R.; Diken, E. G.; Johnson, M. A.; Horvath, S.; McCoy, A. B. Prying Apart a Water Molecule With Anionic H-Bonding: A Comparative Spectroscopic Study of the X⁻·H₂O (X = OH, O, F, Cl, and Br) Binary Complexes in the 600–3800 cm⁻¹ Region. *J. Phys. Chem. A* **2006**, *110*, 4943–4952.
- (36) Majumdar, D.; Kim, J.; Kim, K. S. Charge Transfer to Solvent (CTTS) Energies of Small $X^-(H_2O)_{n=1-4}$ (X = F, Cl, Br, I) Clusters: Ab Initio Study. *J. Chem. Phys.* **2000**, *112*, 101–105.
- (37) Cametti, M.; Dalla Cort, A.; Bartik, K. Fluoride Binding in Water: A New Environment for a Known Receptor. *ChemPhysChem* **2008**, *9*, 2168–2171.
- (38) Bryce, R. A.; Vincent, M. A.; Hillier, I. H. Binding Energy of F (H₂O)-and the Simulation of Fluoride Water Clusters Using a Hybrid QM/MM (Fluctuating Charge) Potential. *J. Phys. Chem. A* **1999**, *103*, 4094–4100.
- (39) Mao, Y.; Demerdash, O.; Head-Gordon, M.; Head-Gordon, T. Assessing Ion-Water Interactions in the AMOEBA Force Field Using Energy Decomposition Analysis of Electronic Structure Calculations. *J. Chem. Theory Comput.* **2016**, *12*, 5422–5437.
- (40) Demerdash, O.; Mao, Y.; Liu, T.; Head-Gordon, M.; Head-Gordon, T. Assessing Many-Body Contributions to Intermolecular Interactions of the AMOEBA Force Field Using Energy Decomposition Analysis of Electronic Structure Calculations. *J. Chem. Phys.* **2017**, *147*, 161721.
- (41) Demerdash, O.; Wang, L.-P.; Head-Gordon, T. Advanced Models for Water Simulations. *Wiley Interdiscip. Rev.: Comput. Mol. Sci.* **2018**, *8*, e1355.
- (42) Ge, Q.; Mao, Y.; Head-Gordon, M. Energy Decomposition Analysis for Exciplexes Using Absolutely Localized Molecular Orbitals. J. Chem. Phys. 2018, 148, 064105.
- (43) Thirman, J.; Head-Gordon, M. Efficient Implementation of Energy Decomposition Analysis for Second-Order Møller-Plesset Perturbation Theory and Application to Anion- π Interactions. *J. Phys. Chem. A* **2017**, *121*, 717–728.
- (44) Loipersberger, M.; Lee, J.; Mao, Y.; Das, A. K.; Ikeda, K.; Thirman, J.; Head-Gordon, T.; Head-Gordon, M. Energy Decomposition Analysis for Interactions of Radicals: Theory and Implementation at the MP2 Level With Application to Hydration of Halogenated Benzene Cations and Complexes between CO₂⁻· and Pyridine and Imidazole. *J. Phys. Chem. A* **2019**, *123*, 9621–9633.
- (45) Ang, S. J.; Mak, A. M.; Wong, M. W. Nature of Halogen Bonding Involving π -systems, Nitroxide Radicals and Carbenes: A Highlight of the Importance of Charge Transfer. *Phys. Chem. Chem. Phys.* **2018**, 20, 26463–26478.
- (46) Su, P.; Tang, Z.; Wu, W. Generalized Kohn-Sham Energy Decomposition Analysis and its Applications. *Wiley Interdiscip. Rev.: Comput. Mol. Sci.* **2020**, *10*, e1460.
- (47) McQuarrie, D. A. Statistical Mechanics; University Science Books: Sausalito, CA, 2000.
- (48) Feyereisen, M. W.; Feller, D.; Dixon, D. A. Hydrogen Bond Energy of the Water Dimer. J. Phys. Chem. 1996, 100, 2993–2997.
- (49) Scheiner, S. Ab Initio Studies of Hydrogen Bonds: The Water Dimer Paradigm. *Annu. Rev. Phys. Chem.* **1994**, *45*, 23–56.
- (50) Reed, A. E.; Weinhold, F. Natural Bond Orbital Analysis of Near-Hartree-Fock Water Dimer. *J. Chem. Phys.* **1983**, *78*, 4066–4073.

- (51) Xu, X.; Goddard, W. A. Bonding Properties of the Water Dimer: A Comparative Study of Density Functional Theories. *J. Phys. Chem. A* **2004**, *108*, 2305–2313.
- (52) Ruscic, B. Active Thermochemical Tables: Water and Water Dimer. J. Phys. Chem. A 2013, 117, 11940–11953.
- (53) Kumagai, T.; Kaizu, M.; Hatta, S.; Okuyama, H.; Aruga, T.; Hamada, I.; Morikawa, Y. Direct Observation of Hydrogen-Bond Exchange Within a Single Water Dimer. *Phys. Rev. Lett.* **2008**, *100*, 166101.
- (54) Ch'ng, L. C.; Samanta, A. K.; Czakó, G.; Bowman, J. M.; Reisler, H. Experimental and Theoretical Investigations of Energy Transfer and Hydrogen-Bond Breaking in the Water Dimer. *J. Am. Chem. Soc.* **2012**, *134*, 15430–15435.
- (55) Ronca, E.; Belpassi, L.; Tarantelli, F. A Quantitative View of Charge Transfer in the Hydrogen Bond: The Water Dimer Case. *ChemPhysChem* **2014**, *15*, 2682–2687.
- (56) Khaliullin, R. Z.; Bell, A. T.; Head-Gordon, M. Electron Donation in the Water-Water Hydrogen Bond. *Eur. J. Chem.* **2009**, *15*, 851–855.
- (57) De Silva, P.; Korchowiec, J. Energy Partitioning Scheme Based on Self-Consistent Method for Subsystems: Populational Space Approach. *J. Comput. Chem.* **2011**, 32, 1054–1064.
- (58) Mukhopadhyay, A.; Xantheas, S. S.; Saykally, R. J. The Water Dimer II: Theoretical Investigations. *Chem. Phys. Lett.* **2018**, 700, 163–175.
- (59) Patra, K.; Ansari, S. A.; Mohapatra, P. K. Metal-Organic Frameworks as Superior Porous Adsorbents for Radionuclide Sequestration: Current Status and Perspectives. *J. Chromatogr. A* **2021**, *1655*, 462491.
- (60) Sabherwal, H.; Tewatia, A.; Kumar, S. S.; Singh, M.; Kataria, N. Metal—Organic Frameworks for Capturing Carbon Dioxide from Flue Gas. *ACS Symp. Ser.* **2021**, *1393*, 355–391.
- (61) Jaramillo, D. E.; Jiang, H. Z.; Evans, H. A.; Chakraborty, R.; Furukawa, H.; Brown, C. M.; Head-Gordon, M.; Long, J. R. Ambient-Temperature Hydrogen Storage via Vanadium(II)-Dihydrogen Complexation in a Metal-Organic Framework. *J. Am. Chem. Soc.* **2021**, *143*, 6248–6256.
- (62) Chakraborty, R.; Carsch, K. M.; Jaramillo, D. E.; Yabuuchi, Y.; Furukawa, H.; Long, J. R.; Head-Gordon, M. Prediction of Multiple Hydrogen Ligation at a Vanadium (II) Site in a Metal-Organic Framework. J. Phys. Chem. Lett. 2022, 13, 10471–10478.
- (63) Jaramillo, D. E.; Reed, D. A.; Jiang, H. Z.; Oktawiec, J.; Mara, M. W.; Forse, A. C.; Lussier, D. J.; Murphy, R. A.; Cunningham, M.; Colombo, V.; Shuh, D. K.; Reimer, J. A.; Long, J. R. Selective Nitrogen Adsorption via Backbonding in a Metal-Organic Framework With Exposed Vanadium Sites. *Nat. Mater.* **2020**, *19*, 517–521.
- (64) Denysenko, D.; Grzywa, M.; Jelic, J.; Reuter, K.; Volkmer, D. Scorpionate-Type Coordination in MFU-4l Metal-Organic Frameworks: Small-Molecule Binding and Activation Upon the Thermally Activated Formation of Open Metal Sites. *Angew. Chem., Int. Ed. Engl.* **2014**, 53, 5832–5836.
- (65) Barnett, B. R.; Evans, H. A.; Su, G. M.; Jiang, H. Z. H.; Chakraborty, R.; Banyeretse, D.; Hartman, T. J.; Martinez, M. B.; Trump, B. A.; Tarver, J. D.; et al. Observation of an Intermediate to H₂ Binding in a Metal-Organic Framework. *J. Am. Chem. Soc.* **2021**, 143, 14884–14894.
- (66) Mardirossian, N.; Head-Gordon, M. ω B97M-V: A Combinatorially Optimized, Range-Separated Hybrid, Meta-GGA Density Functional With VV10 Nonlocal Correlation. *J. Chem. Phys.* **2016**, 144, 214110.
- (67) Weigend, F.; Ahlrichs, R. Balanced Basis Sets of Split Valence, Triple Zeta Valence and Quadruple Zeta Valence Quality for H to Rn: Design and Assessment of Accuracy. *Phys. Chem. Chem. Phys.* **2005**, *7*, 3297
- (68) Khaliullin, R. Z.; Bell, A. T.; Head-Gordon, M. Analysis of Charge Transfer Effects in Molecular Complexes Based on Absolutely Localized Molecular Orbitals. *J. Chem. Phys.* **2008**, *128*, 184112.
- (69) Veccham, S. P.; Lee, J.; Mao, Y.; Horn, P. R.; Head-Gordon, M. A Non-Perturbative Pairwise-Additive Analysis of Charge Transfer

Contributions to Intermolecular Interaction Energies. *Phys. Chem. Chem. Phys.* **2021**, 23, 928–943.

- (70) Shen, H.; Wang, Z.; Head-Gordon, M. Generalization of ETS-NOCV and ALMO-COVP Energy Decomposition Analysis to Connect any Two Electronic States and Comparative Assessment. *J. Chem. Theory Comput.* **2022**, *18*, 7428–7441.
- (71) Lavrich, D. J.; Wetterer, S. M.; Bernasek, S. L.; Scoles, G. Physisorption and Chemisorption of Alkanethiols and Alkyl Sulfides on Au (111). *J. Phys. Chem. B* **1998**, *102*, 3456–3465.
- (72) Epifanovsky, E.; Gilbert, A. T.; Feng, X.; Lee, J.; Mao, Y.; Mardirossian, N.; Pokhilko, P.; White, A. F.; Coons, M. P.; Dempwolff, A. L.; et al. Software for the Frontiers of Quantum Chemistry: An Overview of Developments in the Q-Chem 5 Package. *J. Chem. Phys.* **2021**, 155, 084801.

TRECOMMENDED Recommended by ACS

Graphic Characterization and Clustering Configuration Descriptors of Determinant Space for Molecules

Lei Sun, Ji Chen, et al.

APRIL 03, 2023

JOURNAL OF CHEMICAL THEORY AND COMPUTATION

READ 🗹

Merging the Energy Decomposition Analysis with the Interacting Quantum Atoms Approach

Martí Gimferrer, Pedro Salvador, et al.

MAY 29, 2023

JOURNAL OF CHEMICAL THEORY AND COMPUTATION

READ 🗹

Force Decomposition Analysis: A Method to Decompose Intermolecular Forces into Physically Relevant Component Contributions

Abdulrahman Aldossary, Martin Head-Gordon, et al.

FEBRUARY 08, 2023

THE JOURNAL OF PHYSICAL CHEMISTRY A

READ 🗹

Characterizing Interfaces by Voronoi Tessellation

Daniel Konstantinovsky, Sharon Hammes-Schiffer, et al.

JUNE 02, 2023

THE JOURNAL OF PHYSICAL CHEMISTRY LETTERS

READ 🗹

Get More Suggestions >